



# Dendritic mesoporous silica composite ionic liquid gel polymer electrolyte improves the performance of lithium battery

Huizhe Niu<sup>1</sup> · Nan Zhang<sup>2</sup> · Minling Ding<sup>1</sup> · Xin Li<sup>1</sup> · Xiangyu Su<sup>1</sup> · Xulong Guo<sup>1</sup> · Ping Guan<sup>1</sup> · Xiaoling Hu<sup>1</sup>

Received: 5 March 2022 / Revised: 25 April 2022 / Accepted: 10 May 2022 / Published online: 6 June 2022  
© The Author(s), under exclusive licence to Springer-Verlag GmbH Germany, part of Springer Nature 2022

## Abstract

The application of polymer electrolytes exists the problems of low room temperature ionic conductivity ( $< 10^{-4} \text{ S}\cdot\text{cm}^{-1}$ ) and high electrodes/electrolytes interface impedance. To solve the problems, one dendritic mesoporous silica nanoparticle (DMSN) is synthesized and added in gel polymer electrolyte (GPE) prepared by introduced the imidazole-based ionic liquid ([BMIM]TFSI) in polymer electrolytes based on polyvinylidene fluoride (PVDF) and lithium salt (LiTFSI) to form a composite polymer electrolyte (GPE@SiO<sub>2</sub>). With the DMSN, the ionic conductivity of GPE@SiO<sub>2</sub> is elevated from  $1.86 \times 10^{-4}$  to  $2.47 \times 10^{-4} \text{ S}\cdot\text{cm}^{-1}$  and the tensile strength is also heightened. Moreover, Li/GPE@SiO<sub>2</sub>/LiFePO<sub>4</sub> battery with optimal electrolyte delivers higher discharge capacity of  $138.33 \text{ mAh}\cdot\text{g}^{-1}$  than Li/GPE/LiFePO<sub>4</sub> battery with discharge capacity of  $105.88 \text{ mAh}\cdot\text{g}^{-1}$  at 0.2C. The results indicate that the introduction of ionic liquids and DMSN can synergistically enhance the ionic conductivity, mechanical strength, and electrochemical performance of PVDF-based polymer electrolytes for lithium battery.

**Keywords** Lithium battery · Polymer electrolyte · Ionic liquid · Silica nanoparticles

## Introduction

Lithium batteries have attracted widespread attention in the fields of consumer electronics and electric vehicles due to their high energy density, high output voltage, stable cycle capacity [1–3]. However, lithium batteries in the market mainly use flammable and volatile traditional liquid organic carbonates in electrolytes. Under extreme conditions like heating and overcharging, safety problems such as electrolyte leakage and fire are probable to occur. Besides, lithium

dendrites formed by irregular lithium metal depositing will also increase the risk of thermal runaway [4–6]. Therefore, the development of a novel high-safety electrolyte has been regarded as one of the most effective solutions to solve the safety problems of lithium batteries [7, 8].

Recently, the emergence of solid polymer electrolytes based on polymers such as polyvinylidene fluoride-hexafluoropropylene (PVDF-HFP) [9–11], polyethylene oxide (PEO) [12–14], polymethyl methacrylate (PMMA) [15–17] and polyvinylidene fluoride (PVDF) [18–21], and even lignocellulose (LC) and potato starch [22, 23], have good advantages of film-forming, flexibility, stable electrolyte/electrode interface and easy fabrication [5, 24]. However, due to the low ionic conductivity ( $< 10^{-4} \text{ S}\cdot\text{cm}^{-1}$ ) and high interface impedance between the electrode/electrolyte at room temperature, the solid polymer electrolyte still hard meet the practical demand of lithium-ion batteries [25, 26]. For example, Armand [27] et al. reported that the ionic conductivity of the PEO-based polymer electrolyte for lithium-ion batteries is only  $10^{-5} \text{ S}\cdot\text{cm}^{-1}$  at 40 °C. Thus, it was found in later studies that strategies such as adding plasticizers, introducing inorganic nanofillers, synthesizing block copolymers, and cross-linking can significantly improve the practical problems of polymer electrolytes [21, 28–34].

✉ Nan Zhang  
zhangn123@126.com

✉ Ping Guan  
guanping1113@nwpu.edu.cn

✉ Xiaoling Hu  
huxl@nwpu.edu.cn

<sup>1</sup> The Key Laboratory of Space Applied Physics and Chemistry, School of Chemistry and Chemical Engineering, Northwestern Polytechnical University, Xi'an 710129, People's Republic of China

<sup>2</sup> School of Chemistry and Chemical Engineering, Xi'an University of Science and Technology, Xi'an 710054, People's Republic of China

The preparation of gel polymer electrolyte (GPE) by adding liquid plasticizer can increase the ionic conductivity of polymer electrolyte and further improve its flexibility and electrolyte/electrode interface contact [35–37]. As the plasticizers of many polymer electrolytes, imidazole-based ionic liquid (IL) with high ionic conductivity at room temperature, high chemical and thermal stability, wide electrochemical window, and good plasticizing ability is prospective candidate material [25, 38–41]. For example, Huang [42] et al. doped IL ([BMIM]BF<sub>4</sub>) into PVDF-HFP polymer matrix and successfully prepared IL composite polymer electrolyte with ionic conductivity as high as  $5.26 \times 10^{-4} \text{ S}\cdot\text{cm}^{-1}$  by casting method. However, adding IL into GPE for improving ionic conductivity will decrease the mechanical strength. Fortunately, it is reported that the introduction of inorganic fillers that can be uniformly dispersed into the polymer matrix can simultaneously improve the ionic conductivity of the polymer electrolyte and effectively improve its thermal stability and mechanical properties [43–47]. The results of Chiang [48] et al. showed that TiO<sub>2</sub> nanotube blended with polymer electrolyte can form a composite polymer electrolyte which shows good mechanical strength, and its complex structure can significantly improve the ionic conductivity of the PVDF/LiPF<sub>6</sub> polymer electrolyte.

To obtain one PVDF-based polymer electrolyte with more excellent comprehensive performance, we used IL ([BMIM]TFSI) as a plasticizer to prepared a gel polymer electrolyte (GPE) based on PVDF matrix by casting method. The effect of IL on the performance of GPE was explored by adjusting the content of IL in GPE and further confirmed the optimal ratio. Although the ionic conductivity of GPE was improved with addition of IL, the mechanical strength decreased. For further improving the ionic conductivity and mechanical strength of polymer electrolyte, inorganic nanofillers (dendritic mesoporous silica nanoparticles, DMSN) with special structures were introduced into the as-prepared

GPE to fabricate a composite polymer electrolyte (GPE@SiO<sub>2</sub>) as shown in Fig. 1. The influences of DMSN on the physical and electrochemical properties of GPE@SiO<sub>2</sub> were also discussed. Finally, the GPE@SiO<sub>2</sub> with optimal components was used to assemble Li/LiFePO<sub>4</sub> battery to evaluate its charge–discharge rate capability and cycle performance.

## Experiments

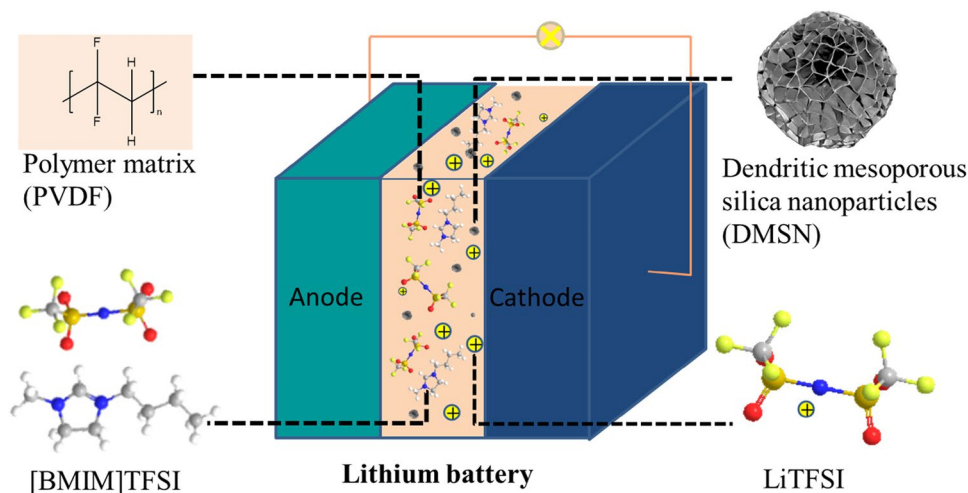
### Materials

N-Methylimidazole (99%), n-Butyl bromide (98%), bis(trifluoromethylsulfonyl)imide lithium (LiTFSI, 99.0%), Tetraethyl orthosilicate (TEOS, 98%), Sodium salicylate (99%), Poly(vinylidene fluoride) (PVDF, average  $M_w$  400,000), (3-Chloropropyl) trimethoxysilane (CP, 99%), imidazole (98%) were purchased from Shanghai Macklin Biochemical Co. Ltd. (Shanghai, China). Ethyl acetate (99%), Hexadecyltrimethylammonium bromide (CTAB, 99%), Triethanolamine (TEA, 85%), Ethanol (99%), N, N-Dimethylformamide (DMF, 99.5%), hydrochloric acid (HCl, 12 mol L<sup>-1</sup>), methylbenzene (98%) were provided by Guangdong Guanghua Sci-Tech Co., Ltd. (Guangdong, China).

### Preparation of PVDF-based ionic liquid gel polymer electrolyte (GPE)

In this study, a solution casting method was used to prepare PVDF based GPE (PVDF + 25% LiTFSI) + X wt.% ([BMIM]TFSI) (where X = 0, 20, 40, 60, 80 and 100). Firstly, PVDF (1.0 g) was dissolved into 8 ml of DMF and stirred magnetically until a homogeneous solution was obtained. Then, LiTFSI (250 mg) was dissolved in 2 ml of DMF to form 0.45 M solution which was slowly added dropwise to the

**Fig. 1** Schematic illustration of GPE@SiO<sub>2</sub>



above homogeneous solution with continued magnetic stirring to mix uniformity. Subsequently, different mass fractions of IL ([BMIM]TFSI) (0%, 20%, 40%, 60%, 80%, and 100%) were mixed in the above-obtained uniform solution, and a series of light yellow uniform solutions were obtained after magnetic stirring for 18 h. Finally, GPE with different content of IL were obtained after vacuum drying at 60 °C for 24 h followed the light yellow uniform solutions were casted on glass plate. According to the content of the added ionic liquid, the prepared GPE membranes were named GPE-0%, GPE-20%, GPE-40%, GPE-60%, GPE-80%, and GPE-100% respectively.

### Preparation of dendritic mesoporous silica nanoparticles (DMSN) inorganic filler

For preparation of DMSN inorganic filler, cetyltrimethylammonium bromide (CTAB) was used as the surfactant. Firstly, TEA (0.27 g) was dissolved in deionized water (100 ml) in a flat-bottomed flask with magnetic stirring for 0.5 h at 80 °C. Subsequently, sodium salicylate (0.67 g) and CTAB (1.52 g) were added to the above solution and stirring was continued for 1 h. Then, the solution gradually changed from clear to turbid after addition of ethyl orthosilicate (TEOS, 16 ml) with stirring at 80 °C. The product was collected by high-speed centrifugation and washed alternately with deionized water and ethanol to remove residual reactants. To remove the surfactant CTAB, the washed product was dispersed in a mixed solution of hydrochloric acid and ethanol (HCl: Ethanol = 1: 9) with stirred at 80 °C followed by centrifugal separation, then washed alternately with deionized water and ethanol for 2~3 times. The final product-dendritic mesoporous silica nanoparticles (DMSN) which present as white powder were obtained after vacuum drying at 60 °C.

### Preparation of DMSN composite PVDF-based ionic liquid GPE (GPE@SiO<sub>2</sub>)

On the basis of GPE-80%, GPE@SiO<sub>2</sub> electrolytes were prepared by introducing DMSN as the inorganic filler. Firstly, PVDF (1.00 g), LiTFSI (0.25 g) and [BMIM]TFSI (0.80 g) were successively dissolved in DMF with magnetic stirring at 45 °C to obtain a homogeneous solution which contains  $9 \times 10^{-4}$  mol LiTFSI in 1 g PVDF polymer matrix. Then, different mass of DMSN, which are 0 wt.%, 5 wt.%, 10 wt.% and 15 wt.% relative to PVDF, were evenly dispersed in DMF solution under the condition of magnetic stirring at 45 °C for 24 h to form uniform slurries. Finally, translucent GPE@SiO<sub>2</sub> electrolytes were obtained after vacuum drying at 60 °C for 48 h followed the uniform slurries were casted on glass plates. According to the mass fractions of the added DMSN inorganic filler, the as-prepared composite GPE@

SiO<sub>2</sub> electrolytes were named GPE-80%, GPE@SiO<sub>2</sub>-5%, GPE@SiO<sub>2</sub>-10% and GPE@SiO<sub>2</sub>-15%, respectively.

### Characterization of material structure and physical and chemical properties

TENSOR infrared spectrometer (Bruker, Germany) was utilized to record the infrared spectrum (FT-IR) of DMSN, providing information on its chemical structure and valence bonds. The microscopic morphology of DMSN and the surface morphology of the GPE were investigated by scanning electron microscopy (SEM, FEI Quanta 400 FEG). The detailed internal structures of DMSN were performed by high-resolution transmission electron microscopy (TEM, Talos F200X, FEI). The crystal structure of GPE was determined by X-Ray diffractometer (XRD, D2 PHASER X, Bruker). The particle size of DMSN was analyzed by the ZEN3690 Zeta sizer Nano detector (Malvern, UK). The specific surface area and pore size distribution were characterized by Brunauer–Emmett–Teller (BET) isothermal nitrogen adsorption–desorption test. The thermal decomposition behavior and phase transition temperature of polymer electrolyte were studied by thermogravimetric analyzer (TGA) and differential scanning calorimeter (DSC). And the mechanical properties of polymer electrolyte were identified by an electronic universal testing machine (INSTRON 3342, Instron, USA).

### The electrochemical properties of GPE

The as-prepared polymer electrolyte membranes were cut into circular shape with the diameter of 19 mm for following testing. All the electrochemical tests were conducted on the CS350H electrochemical work station system (Wuhan Corrtest Instruments Corp., Ltd, China).

#### (1) Ionic conductivity

The electrolyte samples for measurement were sandwiched between two stainless steel electrodes (SS) to assemble SS/electrolyte/SS symmetrical CR2032 coin cells. The AC impedance spectroscopy (EIS) was recorded by the electrochemical work station with AC amplitude of 10 mV between the scan frequency range of 100 kHz-0.1 Hz at the temperature of 20 °C, 30 °C, 40 °C, 50 °C, 60 °C, 70 °C and 80 °C respectively. According to formula (1), the ionic conductivity ( $\sigma$ ) of the electrolyte membrane can be calculated,

$$\sigma = \frac{L}{R_b \times S} \quad (1)$$

where  $R_b$  is the bulk impedance ( $\Omega$ ) obtained from EIS;  $L$  is the thickness (cm) of electrolyte membrane;

$S$  is the contact area of the stainless steel electrode and electrolyte membrane ( $\text{cm}^2$ ).

(2) Ionic migration activation energy

The ionic conduction in the polymer electrolyte mainly occurs in the amorphous region above the glass transition temperature, so the effect of temperature on the transportation of ions in the polymer is noteworthy. The Arrhenius Eq. (2) was performed to describe the temperature dependence of ionic conductivity in polymer electrolytes.

$$\sigma(T) = \sigma_0 \exp\left(\frac{-E_a}{kT}\right) \quad (2)$$

In the formula,  $\sigma_0$  represents the pre-exponential factor which is related to the number of carriers,  $T$  is the thermodynamic temperature,  $k$  is the Boltzmann constant, and  $E_a$  is the activation energy for ionic migration. The lower the activation energy indicates the lower the energy barrier for ion transportation in the system, which contributes to higher ionic conductivity. The activation energy ( $E_a$ ) can be calculated by formula (3) and (4) as follows.

$$\lg \sigma = \lg \sigma_0 - \frac{E_a}{-2.303 \times 1000R} \times \frac{1000}{T} \quad (3)$$

$$k = \frac{E_a}{-2.303 \times 1000R} \quad (4)$$

where,  $k$  is the slope of the obtained straight line by fitting,  $R$  is the gas constant.

(3) Electrochemical stability

Linear sweep voltammetry (LSV) was used to measure the electrochemical stability of the electrolyte. The electrolyte membrane was assembled into a SS/electrolyte membrane/Li asymmetric testing cell with SS as work electrode and lithium metal electrode (Li) as counter and reference electrode. The SS/electrolyte membrane/Li asymmetric testing cell was tested on the electrochemical work station from 2.0 V vs.  $\text{Li}^+/\text{Li}$  to 6.0 V vs.  $\text{Li}^+/\text{Li}$  with a scan rate of  $0.1 \text{ mV} \cdot \text{s}^{-1}$ .

(4) Lithium ion transference number

The lithium ion transference number ( $t_{\text{Li}^+}$ ) is a reflection of the current generated from the mobility of  $\text{Li}^+$ . The higher transference number indicates higher efficiency for the  $\text{Li}^+$  transference, and lower polarization would be occurred. The AC impedance coupled with potentiostatic polarization method was used to determine  $t_{\text{Li}^+}$ . For the measurement of  $t_{\text{Li}^+}$ , a Li/electrolyte/Li symmetrical cell was assembled with lithium metal electrode (Li) as work electrode, counter and reference electrode. Potentiostatic polarization of Li/electrolyte/Li symmetrical cell was conducted on the electrochem-

ical work station with a polarization voltage ( $\Delta V$ ) until a steady current ( $I_s$ ) was got. The initial current ( $I_o$ ) was obtained at the initial potentiostatic polarization. Before and after the potentiostatic polarization, the EIS were conducted to get the impedance before polarization ( $R_o$ ) and after polarization ( $R_s$ ) respectively. The  $t_{\text{Li}^+}$  can be calculated by formula (4):

$$t_{\text{Li}^+} = \frac{I_s(\Delta V - I_o R_o)}{I_o(\Delta V - I_s R_s)} \quad (4)$$

(5) Interfacial stability

The interfacial stability between lithium metal electrode (Li) and electrolyte is estimated by EIS. The Li/electrolyte/Li symmetrical cell was assembled and tested on the electrochemical work station with 10 mV of amplitude in the scan frequency range of 100 kHz–0.1 Hz at the temperature of  $20^\circ \text{C}$  after different storage time. The change of interface impedance with storage time obtained from EIS could be used to evaluate the interfacial stability between lithium metal electrode (Li) and electrolyte.

## The performance of Li/LiFePO<sub>4</sub> battery

For testing the battery performance, Li/electrolyte/LiFePO<sub>4</sub> CR2032 coin batteries are assembled with as-prepared polymer electrolytes, lithium anode and LiFePO<sub>4</sub> cathode which prepared by coating 80 wt.% LiFePO<sub>4</sub>, 10 wt.% carbon black and 10 wt.% PVDF on an aluminum foil and tested on a battery test system (Shenzhen Neware Technology Limited., China). The rate performance of Li/electrolyte/LiFePO<sub>4</sub> was performed between 2.5 V and 4.2 V vs.  $\text{Li}^+/\text{Li}$  at different charge/discharge current density of 0.1C, 0.2C, 0.5C and 1.0C at room temperature. The charge–discharge cycle performance for Li/electrolyte/LiFePO<sub>4</sub> is conducted between 2.5 V–4.2 V vs.  $\text{Li}^+/\text{Li}$  at the current density of 0.2C at room temperature.

## Results and discussion

### Physicochemical properties of inorganic filler dendritic mesoporous silica nanoparticle (DMSN)

It can be clearly seen from the SEM and TEM images of Fig. 2a–d that DMSN owns dendritic structure and uniform particle size with an average particle size of about 250 nm. The uniform particle size and dendritic structure with large specific surface area of DMSN is favourable for using in electrolyte to improve performance. Comparing with other silica nanoparticles [49], although the particle size of DMSN is bigger, but the porous structure, which contains abundant



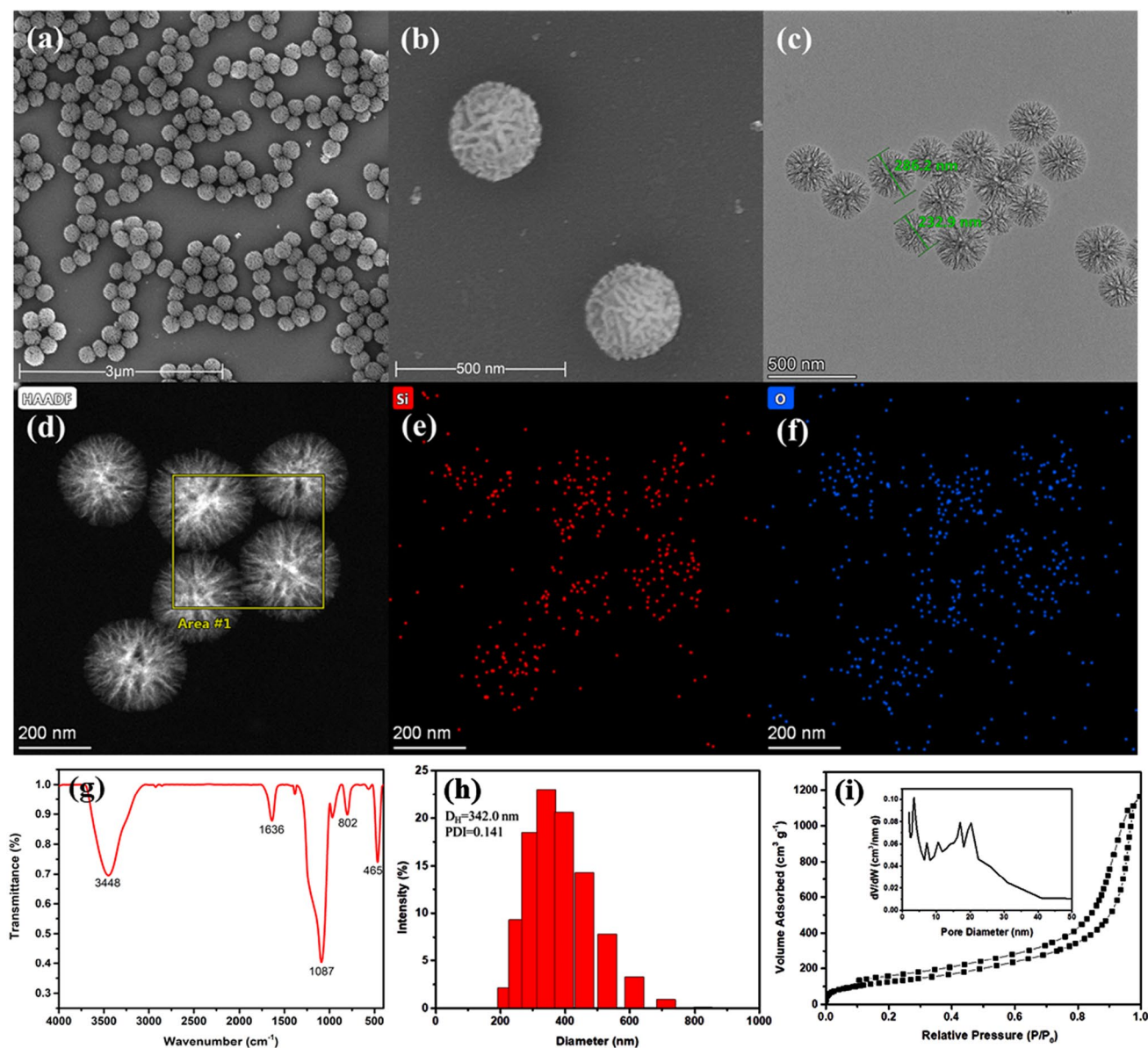


**Fig. 2** a, b SEM images of DMSN; c, d TEM images of DMSN; e, f The element distribution Si and O; g FT-IR spectrum of DMSN; h The chart of DMSN particle size distribution; i Isothermal nitrogen

adsorption and desorption curve of DMSN (the inset showed the pore size distribution diagram)

inter-connective pores, would form a larger number of pathways when liquid electrolyte permeated into the pores for fast migration of  $\text{Li}^+$ . Moreover, from the SEM image of DMSN in Fig. 2b and the TEM images of Fig. 2c, d, it can be seen that the surface of DMSN with dendritic structure is rough and has abundant wrinkled structures caused by the removal of the micelle template. These wrinkled structures contribute to larger specific surface area which avails to enhancing contact area with polymer electrolyte to enhance the mechanical strength polymer electrolyte. Besides providing more channels for lithium ion transmission, the larger specific surface area can also increase the number of

$\text{TFSI}^-$  interacting with DMSN to promote the dissociation of the lithium salt and make more free  $\text{Li}^+$  to participate in conduction for improving ionic conductivity [49–51]. These advantages are beneficial for polymer electrolytes to boost the performance of lithium battery. The energy dispersive X-ray spectroscopy (EDS) of DMSN in Fig. 2e, f only shows Si and O element, which confirms that the template is eluted completely and DMSN has been successfully prepared. Besides, it is can be seen from the FT-IR spectrum of DMSN in Fig. 2g, the absorption peak at  $1087\text{ cm}^{-1}$  is corresponded to the antisymmetric stretching vibration of the Si–O–Si bond, and the strong absorption peaks at

802  $\text{cm}^{-1}$  and 465  $\text{cm}^{-1}$  are related to the symmetric stretching vibration and bending vibration of the Si–O–Si bond in DMSN respectively [52, 53]. The broad absorption peaks at 3448  $\text{cm}^{-1}$  and 1636  $\text{cm}^{-1}$  are ascribed to the asymmetric stretching vibration of the active -OH group on the surface of DMSN. These results also provide evidence for the successful preparation of DMSN. What's more, the asymmetric stretching vibration peak of -CH<sub>2</sub>- of CTAB at 2851  $\text{cm}^{-1}$  is not observed in Fig. 2g, which shows that CTAB had been completely removed during the post-treatment process, and the influence of impurities in the subsequent electrochemical properties study were excluded. The average particle size got from dynamic light scattering (DLS) in Fig. 2h is about 340 nm and is larger than that obtained from SEM and TEM images, which is due to the particle size got from DLS is hydration radius. More importantly, it also can be seen from Fig. 2h that the particle size of DMSN is uniform, which is consistent with the result from Fig. 2a–c. Figure 2i is the isothermal nitrogen adsorption and desorption curve of DMSN. As shown in Fig. 2i and the inset figure, DMSN is a typical IV-type isotherm with an H1 hysteresis ring, and the pore size is mainly distributed around 10.68 nm as shown in Table S1. In addition, the specific surface area of the nanoparticles is as high as 463.88  $\text{m}^2 \text{g}^{-1}$ . The high specific surface area corresponding to the dendritic structure

of DMSN is beneficial to improving the ionic conductivity of polymer electrolyte with DMSN.

### The morphology, structure, mechanical property and ionic conductivity of GPE

The composition, morphology and structure of GPE are critical to its electrochemical performance. Figure 3a shows the photographs of GPE films prepared based on different ionic liquid contents. As seen from the Fig. 3a, the six electrolyte membranes with smooth surface synthesized by adding various proportions of IL ([BMIM]TFSI) are translucent. Figure 3a shows no obvious damage in the photographs of as-prepared GPE with repeated folded-unfold, which reveals that GPE have excellent flexibility and processability. The SEM images of GPE-80% are Fig. 3b and show numerous small pores on the surface, which may be ascribed to swelling of the polymer crosslinking network absorbing a large amount of the IL and phase separation during the evaporation [11, 54]. In consideration of the ionic conductivity is vital to electrolytes, the ionic conductivity of as-prepared GPE are got from their EIS in Fig. S1 and shown in Fig. 3c and Table S2. As shown in Fig. 3c, the ionic conductivity of GPE increases with the increasing of IL until to the maximum value of  $1.57 \times 10^{-4} \text{ S cm}^{-1}$  at the

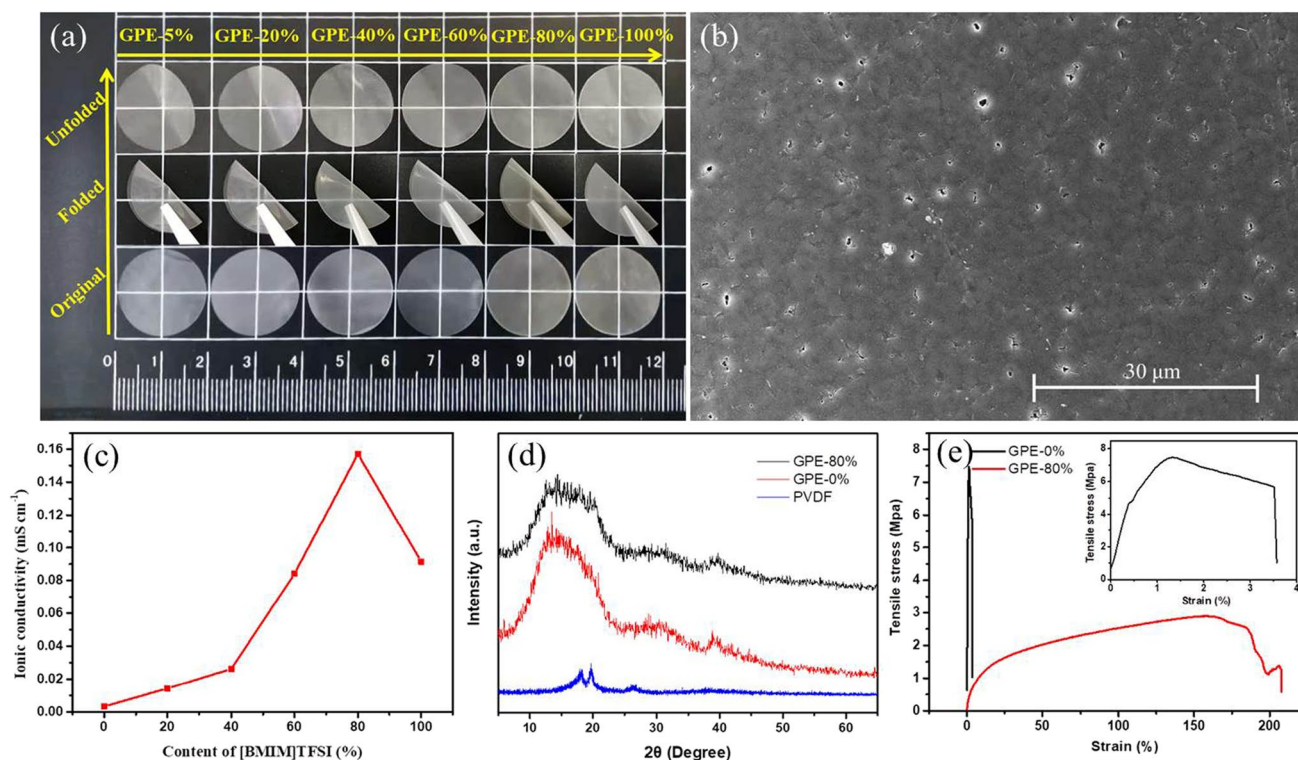


**Fig. 3** a Photographs of PVDF@GPE prepared based on different ionic liquid contents; b The SEM images of GPE-80% electrolyte; c Ion conductivity of GPE with different content of IL ([BMIM]TFSI)

at 20 °C; d XRD patterns of GPE-0% and GPE-80% electrolyte membrane. e Stress–strain curve of GPE (Inset is the enlarged view of GPE-0%)

content of 80% IL, then the ionic conductivity decreases with the increasing of IL. It is due to the increasing content of the IL as plasticizer would increase the consecutive liquid phase in GPE for fast transference of  $\text{Li}^+$ , but the structural integrity of GPE would be destroyed when the content of IL is high enough and the ionic conductivity would be decreased. The GPE is formed by dissolving liquids in polymer matrix, so the mechanical strength of GPE hardly hold their normal function when content of liquids plasticizer is too high, which is responsible for the decrease of ionic conductivity for measurement under some pressure. So the GPE with 80% IL (GPE-80%) is selected for further studies. To further reveal the effect of the IL on GPE, the prepared electrolyte membranes and pristine PVDF power are also analysed by XRD. Figure 3d shows the XRD patterns of pristine PVDF power, GPE-0% and GPE-80% electrolyte membranes. For pristine PVDF power, two small peaks at  $18.5^\circ$  and  $20.1^\circ$  corresponding to  $\alpha$ -phase PVDF appear in XRD pattern [55]. However, as can be seen from Fig. 3d, a wide dispersion peak appears in XRD patterns of GPE-0% and GPE-80%, indicating that the addition of lithium salt (LiTFSI) and IL makes GPE to be amorphous and is favour of movement of PVDF chain segment for improving the ionic conductivity of the electrolyte. Besides, the mechanical strength of GPE will decrease with increasing of IL. As shown in Fig. 3e, the tensile strain of GPE with 80% IL increases from 3.5% to 200%, but the tensile strength falls from 7.5 MPa to 2.89 MPa dramatically. In consideration of the weak mechanical strength of GPE with high ionic conductivity, DMSN is tried to be used to improve mechanical strength and electrochemical performance.

### The morphology, structure, mechanical property, and ionic conductivity of GPE@SiO<sub>2</sub>

Basing on improvement of GPE-80%, DMSN is introduced to prepared SiO<sub>2</sub> composite polymer electrolyte membranes (GPE@SiO<sub>2</sub>) and named them as GPE-80%, GPE@SiO<sub>2</sub>-5%, GPE@SiO<sub>2</sub>-10%, GPE@SiO<sub>2</sub>-15% according to the content of DMSN (0 wt.%, 5 wt.%, 10 wt.% and 15 wt.%). The surface photographs of GPE@SiO<sub>2</sub> are shown in Fig. 4a and they are all colorless and translucent. As same as GPE shown in Fig. 3a, GPE@SiO<sub>2</sub> also show no obvious damage after repeatedly folded-unfold in Fig. 4a, revealing excellent flexibility and processability. From the SEM images of GPE@SiO<sub>2</sub>-5% in Fig. 4b, c, it can be seen that DMSN nanoparticles are dispersed in the PVDF matrix and the energy spectrum of Si and O elements for GPE@SiO<sub>2</sub>-5% in Fig. 4d, e also show the existing of DMSN, but the dispersion of DMSN nanoparticles is uneven with a few agglomerations. The ionic conductivity of GPE@SiO<sub>2</sub> calculated from the EIS in Fig. S2 is shown in Fig. 4f and Table S3, which can be got from is that the

ionic conductivity of GPE@SiO<sub>2</sub> is improved to  $2.47 \times 10^{-4} \text{ S cm}^{-1}$  with 5 wt.% DMSN, then it decreases drastically with increasing of DMSN. The improved ionic conductivity for GPE@SiO<sub>2</sub> is most likely due to the DMSN disturb the arrangement of the polymer segment and decrease the crystalline of polymer matrix [49, 56]. Besides, the larger specific surface area of dendritic DMSN which increases anion (TFSI<sup>-</sup>) interacting with the silanol (Si-OH) of DMSN by Lewis acid–base interaction and lets more carriers ( $\text{Li}^+$ ) to participate in conduction [51]. The  $\text{Li}^+$  can move in polymer electrolyte along the channels formed on the surface of DMSN with large specific surface area for fast transmission, which also contributes to the improved ionic conductivity [26, 33, 57, 58]. The improved ionic conductivity of GPE@SiO<sub>2</sub> with 5 wt.% DMSN (GPE@SiO<sub>2</sub>-5%) also can be seen in Fig. 4g. Figure 4g shows that the temperature dependences of ionic conductivity for GPE-80% and GPE@SiO<sub>2</sub>-5% obtained from Figure S3 and S4 all can linear fit with Arrhenius Eq. (3). The activation energy ( $E_a$ ) of GPE@SiO<sub>2</sub>-5% calculated from the slope ( $k = -1.2454$ ) of the fitted line is  $23.74 \text{ kJ mol}^{-1}$  which is lower than that of GPE-80% with a value of  $31.69 \text{ kJ mol}^{-1}$  calculated from the slope ( $k = -1.6538$ ) as displayed in Table S4, indicating that  $\text{Li}^+$  in GPE@SiO<sub>2</sub>-5% transfers more easily than in GPE-80% at low temperature. However, excess DMSN would occur to aggregation due to the large surface energy of DMSN particle, which decreases the specific surface area and hinders the transmission of  $\text{Li}^+$  to decrease the ionic conductivity. Besides, the mechanical strength of GPE@SiO<sub>2</sub> is studied and the results are shown in Fig. 4h. As shown in Fig. 4h, the mechanical strength of GPE@SiO<sub>2</sub> is enhanced with the addition of DMSN and the tensile strength reaches the biggest value of 5.28 Mpa with 15 wt.% DMSN, which is almost 2 times as high as that of GPE-80%. While GPE@SiO<sub>2</sub>-5% obtains a tensile strength of 3.84 MPa and tensile strain of 279.95%, which are also improved much comparing with GPE-80% with a tensile strength of 2.89 MPa and tensile strain of 200%. In view of the highest ionic conductivity and moderate mechanical strength of GPE@SiO<sub>2</sub>-5%, GPE@SiO<sub>2</sub>-5% is used to do following studies. Moreover, it can be seen from Fig. 4i that the XRD pattern of GPE@SiO<sub>2</sub>-5% shows almost a same wide dispersion peak between  $10^\circ$  and  $20^\circ$  as GPE-80%, which indicates that the addition of dendritic mesoporous SiO<sub>2</sub> nanoparticles (DMSN) has no obvious effect on amorphism of GPE@SiO<sub>2</sub>-5%. However, it can be seen from XRD pattern in Figure S5 that the two small peaks at  $18.5^\circ$  and  $20.1^\circ$  for pristine PVDF become weak with addition of DMSN, which is due to the crystalline of PVDF is decreased by adding DMSN filler [59]. The results demonstrate that DMSN also can decrease the crystalline of PVDF to increase the ionic conductivity of polymer electrolyte.



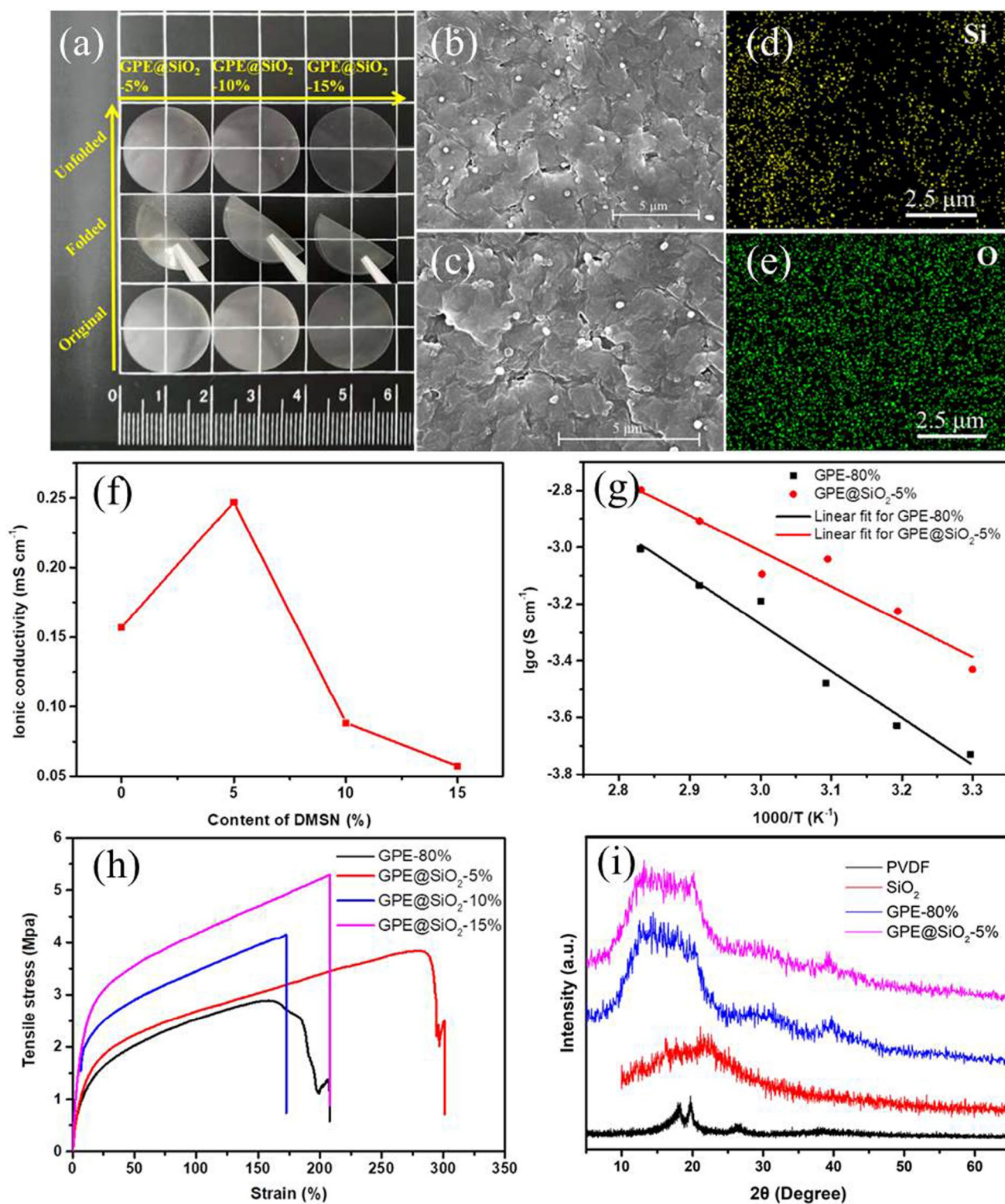


**Fig. 4** a Photographs of GPE@SiO<sub>2</sub>-X% (X=5, 10, 15) composite electrolyte; b, c SEM images of GPE@SiO<sub>2</sub>-5% composite electrolyte; d, e The distribution of Si and O elements in GPE@SiO<sub>2</sub>-5% composite electrolyte; f Ion conductivity of GPE with different con-

tent of IL ([BMIM]TFSI) at 20 °C; g Temperature dependence of ionic conductivity ( $\sigma$ ) and Arrhenius linear fitting of GPE-10% and GPE@SiO<sub>2</sub>-5%; h Stress-strain curve of GPE-80% and GPE@SiO<sub>2</sub>; i XRD patterns of GPE@SiO<sub>2</sub>-X% composite electrolyte



### Thermal stability of electrolytes

The thermal stability of GPE is one of the key indicators to evaluate its safety, which is related to the application of lithium battery in a wide temperature range. TGA and DSC are used to determine the thermal stability of the prepared GPE. As shown as the TGA curve of GPE in Fig. 5a, it can be clearly observed that GPE-80% occurs weight loss between 200–300 °C, which is related to the thermal decomposition of [BMIM]TFSI. The following weight loss between 300–450 °C is attributed to the thermal decomposition of lithium salt LiTFSI and the PVDF matrix [60, 61]. The TGA curve of GPE@SiO<sub>2</sub>-5% is almost same with GPE-80% as shown in Fig. 5a, while the weight loss related to the decomposition of [BMIM]TFSI between 200 and 320 °C and the weight loss attributed to the thermal decomposition of LiTFSI and PVDF between 320 and 450 °C for GPE@SiO<sub>2</sub>-5% are different with GPE-80% [60, 61]. From the result of TGA, the thermal decomposition temperature of as-prepared GPE@SiO<sub>2</sub>-5% is about 200 °C, which can guarantee the safety of lithium battery with GPE@SiO<sub>2</sub>-5% below the temperature of 200 °C. However, as the DSC curves shown in Fig. 5b, there is endothermic peak at around 149 °C for three polymer electrolytes, which is related to the melt of them. The result indicates the GPE-80% and GPE@SiO<sub>2</sub>-5% can keep normal electrochemical properties up to the temperature of 149 °C. In consideration of the improved ionic conductivity and mechanical strength for GPE@SiO<sub>2</sub>-5% with DMSN, the thermal stability unaffected by DMSN is satisfactory result for GPE@SiO<sub>2</sub>-5% applied in lithium battery.

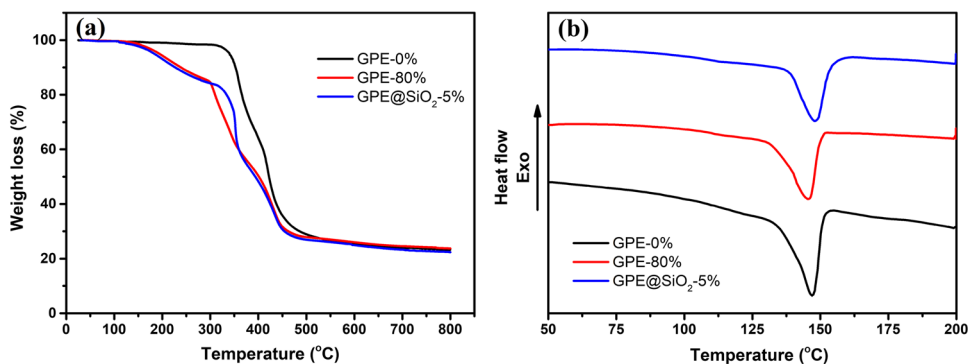
### Electrochemical stability, lithium ion transference number and interfacial stability

The electrochemical stability of electrolytes is often described with the electrochemical window, which determines the operating voltage and energy density of lithium battery. The electrochemical windows of as-prepared polymer electrolytes are obtained by linear sweep voltammetry

(LSV) and the result is shown in Fig. 6a, b. As shown in Fig. 6a, b, there is no obvious current signal in the LSV curves of both electrolytes until the potential higher than 4.3 V vs. Li<sup>+</sup>/Li where the electrochemical oxidation can be occurred for the electrolytes. The limiting oxidation potential of GPE@SiO<sub>2</sub>-5% get from the LSV curves is 4.3 V vs. Li<sup>+</sup>/Li which is a little lower than 4.5 V vs. Li<sup>+</sup>/Li for GPE-80%. The decreased oxidation potential for GPE@SiO<sub>2</sub>-5% may be attributed to the electrochemical oxidation of group on DMSN. The result reveals that the addition of DMSN has an obvious influence on the electrochemical stability of GPE@SiO<sub>2</sub>-5%, and the wide electrochemical windows of GPE-80% and GPE@SiO<sub>2</sub>-5% allow them to be assembled with cathode with moderate voltage, such as LiFePO<sub>4</sub> (LFP) with 3.6 V vs. Li<sup>+</sup>/Li and LiCoO<sub>2</sub> (LCO) with 4.2 V vs. Li<sup>+</sup>/Li, to improve the operating voltage and energy density of lithium battery [62–66].

Lithium ion (Li<sup>+</sup>) transference number ( $t_{Li^+}$ ) can present the efficiency of current produced by transference of Li<sup>+</sup>. The  $t_{Li^+}$  of GPE-80% and GPE@SiO<sub>2</sub>-5% can be obtained from chronoamperometry and ac impedance spectra (EIS), and the results are shown in Fig. 6c, d and Table 1. As the equivalent circuit shown in insets of Fig. 6c, d, the impedance spectra contain semicircles at high frequency and low frequency, which are corresponding to passivation layer resistance ( $R_p$ ) and charge transfer resistance ( $R_{ct}$ ) respectively, and they make up interface resistance ( $R_{int}$ ). The  $R_b$  represents the bulk resistance of electrolyte and its value can be got from the intercept on the real axis at high frequency. As shown in Fig. 6d and Table 1, the initial current ( $I_o$ ) and resistance ( $R_o$ ) before polarization for GPE@SiO<sub>2</sub>-5% are 0.032 mA and 591 Ω, then the steady current ( $I_s$ ) and resistance ( $R_s$ ) after polarization with a polarization voltage ( $\Delta V$ ) become 0.028 mA and 586 Ω. The  $t_{Li^+}$  of GPE@SiO<sub>2</sub>-5% calculated with formula (4) is 0.26 which is smaller than that of GPE-80% with 0.24 got from Fig. 6c. The increased  $t_{Li^+}$  for GPE@SiO<sub>2</sub>-5% is attributed to that the silanol (Si–OH) on the acidic surfaces of DMSN will compete interact with anions (TFSI<sup>-</sup>) of lithium salt by Lewis acid–base interaction, which would lead more lithium salts to dissociate and

Fig. 5 a TGA curve of polymer electrolytes; b DSC curves of polymer electrolytes



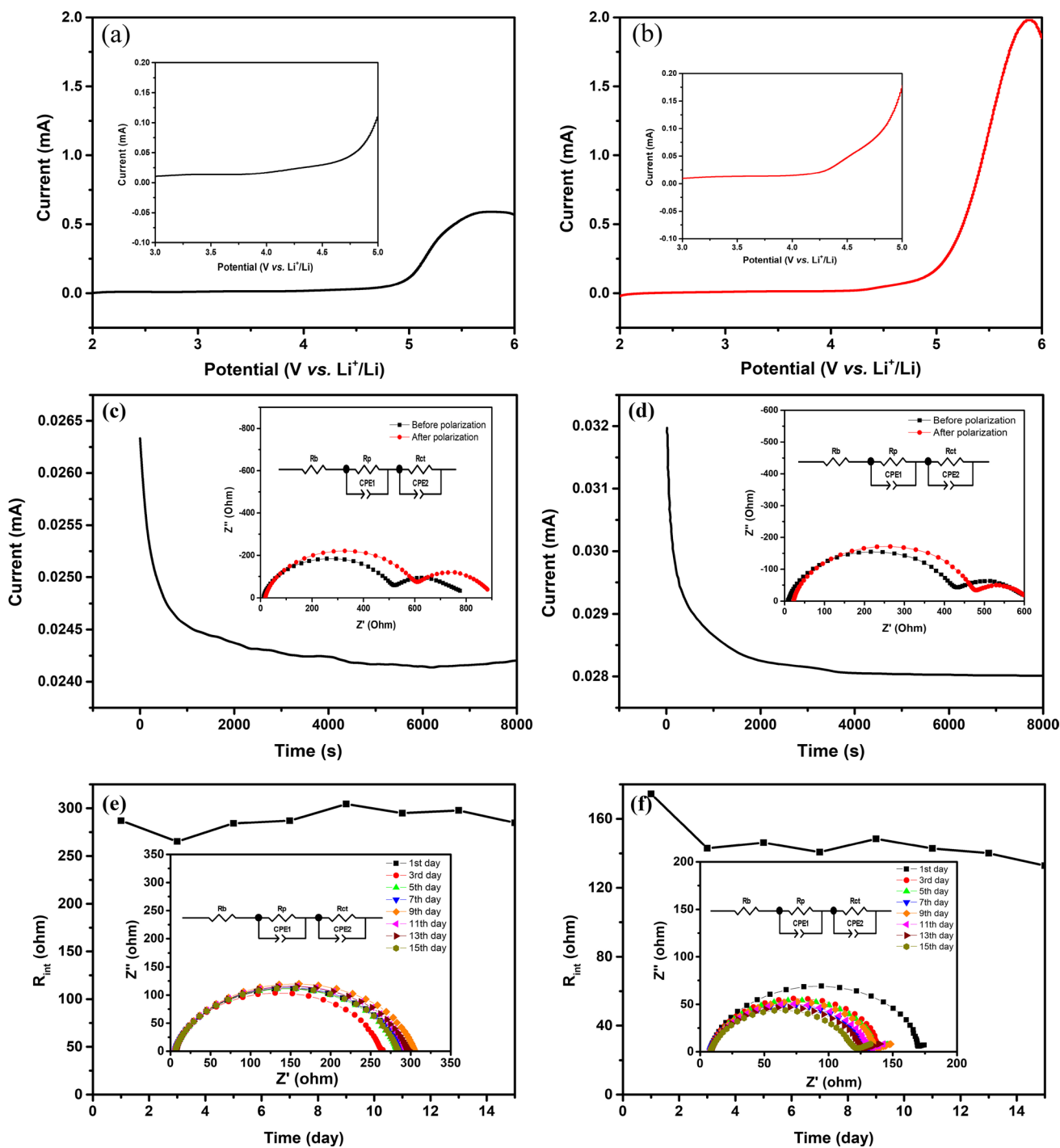


**Fig. 6** LSV curves of as-prepared GPE-80% (a) and GPE@SiO<sub>2</sub>-5% (b); Chronoamperometry curves of GPE-80% (c) and GPE@SiO<sub>2</sub>-5% (d) (Insets are the ac impedance spectra before and after polariza-

tion); Interfacial resistance of Li/GPE-80%/Li (e) and Li/GPE@SiO<sub>2</sub>-5%/Li (f) at different storage time at 20 °C (Inset is AC impedance spectra of Li/GPE/Li after different storage time)

**Table 1** Lithium ion transference number of GPE-80% and GPE@SiO<sub>2</sub>-5%

Sample	$R_o$ ( $\Omega$ )	$R_s$ ( $\Omega$ )	$I_o$ (mA)	$I_s$ (mA)	$\Delta V$ (mV)	$t_{Li^+}$
GPE-80%	770	801	0.02645	0.02423	20	0.24
GPE@SiO <sub>2</sub> -5%	591	586	0.03203	0.02817	20	0.26

free more  $\text{Li}^+$  for conduction [15, 26, 51, 57, 58, 67]. The increasing for  $t_{\text{Li}^+}$  of GPE@ $\text{SiO}_2$ -5% is favorable for decreasing the effect of polarization during the charge–discharge of lithium battery to enhance the capacity and safety.

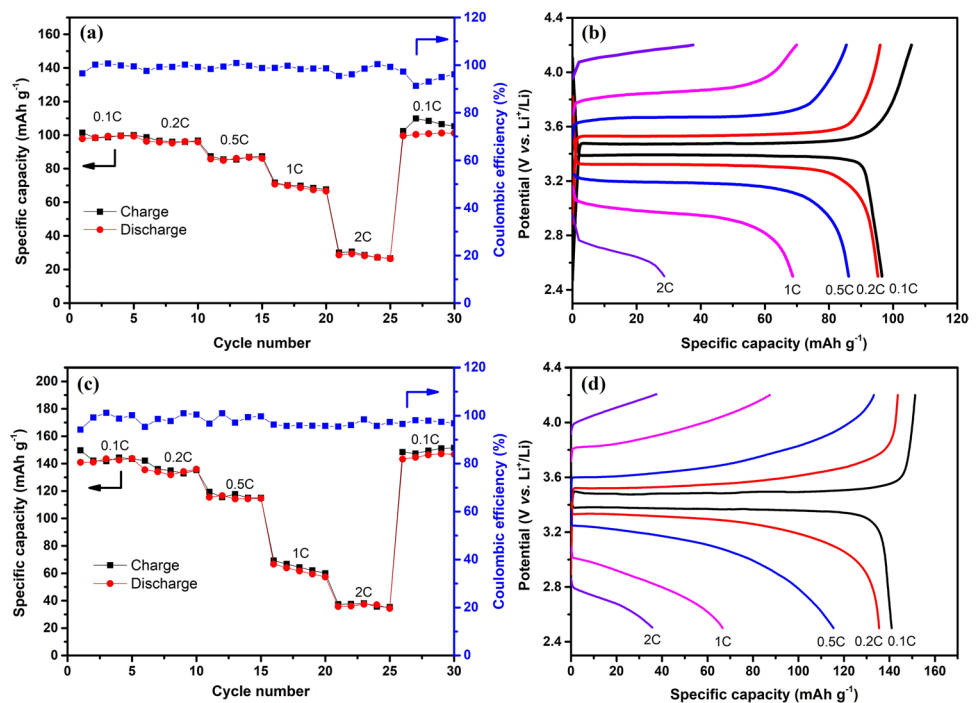
Stable interfacial property between electrolyte and electrode can improve the capacity, safety and performance of lithium battery. Figure 6e, f shows the change of interfacial resistance ( $R_{\text{int}}$ ) for GPE-80% and GPE@ $\text{SiO}_2$ -5%, which can reveal the interfacial stability of electrolyte and lithium electrode. The interfacial resistances are composed of passivation layer resistance ( $R_p$ ) and charge transfer resistance ( $R_{\text{ct}}$ ) as shown in inset of Fig. 6e, f. As shown in Fig. 6e, f, the interfacial resistances of GPE-80% and GPE@ $\text{SiO}_2$ -5% decrease firstly until 3<sup>rd</sup> day, subsequently increase with storage time and finally steady around 284  $\Omega$  and 132  $\Omega$  respectively. The interfacial resistance decreasing in first 3 days is due to the polymer electrolytes infiltrate to electrode, while the increase of interfacial resistance is ascribed to the formation of passivation layer (SEI). The formation of stable passivation layer (SEI) can prevent the irreversible reaction between electrolyte and electrode, which can increase the capacity and suppress the growth of lithium dendrites for improving safety of lithium battery. In the Fig. 6e, it can be seen that the interfacial resistance between GPE-80% and lithium electrode fluctuates with storage time. The interfacial resistances decrease from initial value of 286  $\Omega$  after 3 days storage time, and then it increases obviously to 304  $\Omega$  and steady around 283  $\Omega$  finally. However, as shown in Fig. 6f, the interfacial resistance between GPE@ $\text{SiO}_2$ -5% and lithium electrode decreases from initial value

of 174  $\Omega$  to 142  $\Omega$  after 3 days and has no large fluctuation in the following storage time. The result reveals that the addition of DMSN nanoparticles improves the interfacial property between GPE@ $\text{SiO}_2$ -5% and lithium electrode, which decreases the interfacial resistance and allows form more stable SEI.

### Battery performance

To investigate the performance of the as-prepared polymer electrolytes in lithium batteries, Li/polymer electrolyte/ $\text{LiFePO}_4$  batteries are assembled and their charge–discharge rate and cycle performance are measured. Figure 7 shows the rate performance of Li/GPE-80%/LiFePO<sub>4</sub> battery and Li/GPE@ $\text{SiO}_2$ -5%/LiFePO<sub>4</sub> battery measured at different rates. As shown in Fig. 7a, c, the capacity of batteries decrease with the increase of charge/discharge current density. The discharge capacity of Li/GPE@ $\text{SiO}_2$ -5%/LiFePO<sub>4</sub> battery are 141  $\text{mAh}\cdot\text{g}^{-1}$ , 135  $\text{mAh}\cdot\text{g}^{-1}$ , 115  $\text{mAh}\cdot\text{g}^{-1}$ , 66  $\text{mAh}\cdot\text{g}^{-1}$ , and 35  $\text{mAh}\cdot\text{g}^{-1}$  at discharge current density of 0.1C, 0.2C, 0.5C, 1C, and 2C respectively. Besides, the discharge capacity recover to 143  $\text{mAh}\cdot\text{g}^{-1}$  when the discharge current density return to 0.1C from 2C, showing perfect rate performance. While, Li/GPE-80%/LiFePO<sub>4</sub> battery delivers discharge capacity of 98  $\text{mAh}\cdot\text{g}^{-1}$ , 96  $\text{mAh}\cdot\text{g}^{-1}$ , 85  $\text{mAh}\cdot\text{g}^{-1}$ , 70  $\text{mAh}\cdot\text{g}^{-1}$ , and 29  $\text{mAh}\cdot\text{g}^{-1}$  at discharge current density of 0.1C, 0.2C, 0.5C, 1C, and 2C respectively, and the discharge capacity recover to initial value when the discharge current density return to 0.1C from 2C. The decrease of capacity with the increase of charge/discharge current density is due

**Fig. 7** The charge and discharge specific capacity at different rates (a) and corresponding charge–discharge curves (b) for Li/GPE-80%/LiFePO<sub>4</sub> battery; The charge and discharge specific capacity at different rates (c) and corresponding charge–discharge curves (d) for Li/GPE@SiO<sub>2</sub>-5%/LiFePO<sub>4</sub> battery (The measurements are performed under room temperature)





to the polarization in batteries. As shown in the charge–discharge curves of Fig. 7b, d, the charge plateau and discharge plateau increase and decrease respectively with the increase of current density due to the polarization voltage which can be relieved by improving ionic conductivity and lithium ion transference number. Thank for the high ionic conductivity improved by DMSN filler, the discharge capacities of Li/GPE@SiO<sub>2</sub>-5%/LiFePO<sub>4</sub> batteries at different rate are much higher than that for Li/GPE-80%/LiFePO<sub>4</sub> batteries. In spite of the good rate performance performed by Li/GPE-80%/LiFePO<sub>4</sub> batteries, Li/GPE@SiO<sub>2</sub>-5%/LiFePO<sub>4</sub> batteries assembled with GPE@SiO<sub>2</sub>-5% show higher capacities at same current density and obtain better rate performance.

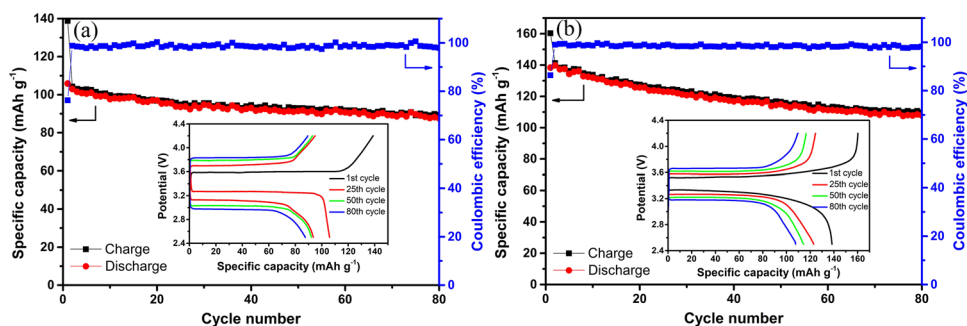
The cycle performance at one certain current density is significant for the cycle life of lithium battery. Figure 8 shows the charge and discharge specific capacity of Li/GPE-80%/LiFePO<sub>4</sub> battery and Li/GPE@SiO<sub>2</sub>-5%/LiFePO<sub>4</sub> battery at different cycle number under current density of 0.2C, and their charge–discharge curves for different cycle number as insets are shown in Fig. 8a, b. As shown in Fig. 8a, the initial specific discharge capacity for Li/GPE-80%/LiFePO<sub>4</sub> battery is 106 mAh g<sup>-1</sup>. After 80 cycles, the discharge capacity of the battery is still as high as 88 mAh g<sup>-1</sup> and the coulombic efficiency is higher than 98%. It can be seen from Fig. 8b that the discharge capacity of Li/GPE@SiO<sub>2</sub>-5%/LiFePO<sub>4</sub> battery for 1<sup>st</sup> cycle is 138 mAh g<sup>-1</sup>. With the increasing of the cycle number, the discharge capacity of Li/GPE@SiO<sub>2</sub>-5%/LiFePO<sub>4</sub> battery decreases to 108 mAh·g<sup>-1</sup> after 80 cycles with a coulombic efficiency closed to 100%. The low coulombic efficiency at 1<sup>st</sup> cycle for both polymer electrolytes is ascribed to the formation of passivation layer (SEI), and a stable SEI would allow the battery to deliver a stable discharge capacity in cycle [68]. As shown in Fig. 8, the discharge capacity of Li/GPE-80%/LiFePO<sub>4</sub> battery is much smaller than that for Li/GPE@SiO<sub>2</sub>-5%/LiFePO<sub>4</sub> battery due to bigger polarization which can be deduced from larger charge potential/smaller discharge potential in insets of Fig. 8. For example, the discharge voltage plateau of 1<sup>st</sup> cycle for Li/GPE@SiO<sub>2</sub>-5%/LiFePO<sub>4</sub> battery is 3.33 V which is higher than that for Li/GPE-80%/LiFePO<sub>4</sub> battery with a value of 3.26 V, which

indicates that the resistance of Li/GPE@SiO<sub>2</sub>-5%/LiFePO<sub>4</sub> battery is less than Li/GPE-80%/LiFePO<sub>4</sub> battery. Small resistance in battery can decrease the effect of polarization on capacity, so the discharge capacity of Li/GPE@SiO<sub>2</sub>-5%/LiFePO<sub>4</sub> battery is larger than Li/GPE-80%/LiFePO<sub>4</sub> battery. Moreover, although the discharge capacity of Li/GPE@SiO<sub>2</sub>-5%/LiFePO<sub>4</sub> battery also decreases obviously in 80 cycles, the rate capacity and cycle capacity in measurement is improved obviously. It is maybe due to the stable passivation layer is formed on the lithium electrode in Li/GPE@SiO<sub>2</sub>-5%/LiFePO<sub>4</sub> battery as shown in Figure S6. The surface optical photographs of lithium electrode in Li/GPE-80%/LiFePO<sub>4</sub> battery with 50 charge–discharge cycles in Figure S6(a) shows that the cracked and rough surface of lithium electrode is maybe due to the severe reaction between electrode and electrolyte, which is responsible to the low discharge capacity and high polarization. While, the surface optical photographs of lithium electrode in Li/GPE@SiO<sub>2</sub>-5%/LiFePO<sub>4</sub> battery with same cycles in Figure S6(b) is coated with one dense layer and the surface of lithium electrode under the dense layer is glossy. The dense layer is related to the formation of passivation layer, which suppresses the reaction between electrode and electrolyte and contributes to higher discharge capacity [59]. So it is feasible that DMSN fillers are introduced into polymer electrolyte to prepare SiO<sub>2</sub> composite polymer electrolyte (GPE@SiO<sub>2</sub>) to improve the energy density of lithium battery with high safety.

## Conclusions

In this study, one dendritic mesoporous silica nanoparticle (DMSN) is prepared and introduced into gel polymer electrolyte (GPE) composed of PVDF matrix, ionic liquid ([BMIM]TFSI) and lithium salt (LiTFSI) to prepared composite gel polymer electrolyte (GPE@SiO<sub>2</sub>). With the introduction of DMSN, the mechanical strength of GPE@SiO<sub>2</sub> can be enhanced 2 times compared with GPE-80% which is the GPE containing 80 wt.% [BMIM]TFSI. GPE@SiO<sub>2</sub>-5% electrolyte with 5 wt.% DMSN obtain an

**Fig. 8** **a** The charge and discharge specific capacity of Li/GPE-80%/LiFePO<sub>4</sub> battery with different cycle number at 0.2C under room temperature; **b** the charge and discharge specific capacity of Li/GPE@SiO<sub>2</sub>-5%/LiFePO<sub>4</sub> battery with different cycle number at 0.2C under room temperature (Insets are charge–discharge curves for different cycle number)



ionic conductivity of  $2.47 \times 10^{-4} \text{ S cm}^{-1}$  which is higher than that of GPE-80% with a value of  $1.57 \times 10^{-4} \text{ S cm}^{-1}$  at 20 °C. However, the effect of DMSN on the thermal and electrochemical stability of GPE@SiO<sub>2</sub>-5% is not obvious. The thermal decomposition temperature of as-prepared GPE@SiO<sub>2</sub>-5% is about 200 °C and the limiting oxidation potential of GPE@SiO<sub>2</sub>-5% is 4.98 V vs. Li<sup>+</sup>/Li which can be assembled with cathode with high voltage to improve the operating voltage, safety and energy density of lithium battery. Moreover, the Li/GPE@SiO<sub>2</sub>-5%/LiFePO<sub>4</sub> battery shows good rate performance and higher rate capacity than Li/GPE-80%/LiFePO<sub>4</sub> battery. Although the stable capacity is delivered by Li/GPE-80%/LiFePO<sub>4</sub> battery under the current density of 0.2C, the Li/GPE@SiO<sub>2</sub>-5%/LiFePO<sub>4</sub> battery obtains higher discharge voltage and capacity than Li/GPE-80%/LiFePO<sub>4</sub> battery. In spite of the severe decrease for the discharge capacity of the Li/GPE@SiO<sub>2</sub>-5%/LiFePO<sub>4</sub> battery, it is feasible that SiO<sub>2</sub> composite polymer electrolyte (GPE@SiO<sub>2</sub>) with DMSN fillers obtains improved ionic conductivity and mechanical strength, which can be used to improve the energy density of lithium battery.

**Supplementary Information** The online version contains supplementary material available at <https://doi.org/10.1007/s11581-022-04609-0>.

**Acknowledgements** Zhang Nan from Xi'an University of Science and Technology is grateful for research start-up fund support of Xi'an University of Science and Technology. The authors from Northwestern Polytechnical University are grateful for the financial support of Shaanxi Province Key R&D Program (2020GY-285). The authors would like to thank Shaanxi Province Key R&D Program leadership, partners, and members for their contributions on this project.

## Declarations

**Conflict of interest** The authors declare no competing interests.

## References

- Zhao H, Yu X, Li J, Li B, Shao H, Li L, Deng Y (2019) Film-forming electrolyte additives for rechargeable lithium-ion batteries: progress and outlook. *J Mater Chem A* 7:8700–8722. <https://doi.org/10.1039/C9TA00126C>
- Kamat PV (2019) Lithium-Ion Batteries and Beyond: Celebrating the 2019 Nobel Prize in Chemistry-A Virtual Issue. *ACS Energy Lett* 4:2757–2759. <https://doi.org/10.1021/acsenenergylett.9b02280>
- Blomgren GE (2017) The development and future of lithium ion batteries. *J Electrochem Soc* 164(1):A5019–A5025. <https://doi.org/10.1149/2.0251701jes>
- Zhang Q, Liu K, Ding F, Liu X (2017) Recent advances in solid polymer electrolytes for lithium batteries. *Nano Res* 10(12):4139–4174. <https://doi.org/10.1007/s12274-017-1763-4>
- Sun C, Liu J, Gong Y, Wilkinson DP, Zhang J (2017) Recent advances in all-solid-state rechargeable lithium batteries. *Nano Energy* 33:363–386. <https://doi.org/10.1016/j.nanoen.2017.01.028>
- Dirican M, Yan C, Zhu P, Zhang X (2019) Composite solid electrolytes for all-solid-state lithium batteries. *Mater Sci Eng R* 136:27–46. <https://doi.org/10.1016/j.mser.2018.10.004>
- Liao Y, Sun C, Hu S, Li W (2013) Anti-thermal shrinkage nanoparticles/polymer and ionic liquid based gel polymer electrolyte for lithium ion battery. *Electrochim Acta* 89:461–468. <https://doi.org/10.1016/j.electacta.2012.11.095>
- Itoh T, Hirata N, Wen Z, Kubo M, Yamamoto O (2001) Polymer electrolytes based on hyperbranched polymers. *J Power Sources* 97–98:637–640. [https://doi.org/10.1016/S0378-7753\(01\)00578-X](https://doi.org/10.1016/S0378-7753(01)00578-X)
- Jie J, Liu Y, Cong L, Zhang B, Lu W, Zhang X, Liu J, Xie H, Sun L (2020) High-performance PVDF-HFP based gel polymer electrolyte with a safe solvent in Li metal polymer battery. *J Energy Chem* 49:80–88. <https://doi.org/10.1016/j.jechem.2020.01.019>
- Tong R-A, Chen L, Fan B, Shao G, Liu R, Wang C-A (2021) Solvent-Free Process for Blended PVDF-HFP/PEO and LLZTO Composite Solid Electrolytes with Enhanced Mechanical and Electrochemical Properties for Lithium Metal Batteries. *ACS Appl Energy Mater* 4(10):11802–11812. <https://doi.org/10.1021/acsaem.1c02566>
- Luo K, Yi L, Chen X, Yang L, Zou C, Tao X, Li H, Wu T, Wang X (2021) PVDF-HFP-modified gel polymer electrolyte for the stable cycling lithium metal batteries. *J Electroanal Chem* 895:115462. <https://doi.org/10.1016/j.jelechem.2021.115462>
- Wang H, Cui X, Zhang C, Gao H, Du W, Chen Y (2020) Promotion of Ionic Conductivity of PEO-Based Solid Electrolyte Using Ultrasonic Vibration. *Polymers* 12(9):1889. <https://doi.org/10.3390/polym12091889>
- Mindemark J, Lacey MJ, Bowden T, Brandell D (2018) Beyond PEO-Alternative host materials for Li<sup>+</sup>-conducting solid polymer electrolytes. *Prog Polym Sci* 81:114–143. <https://doi.org/10.1016/j.progpolymsci.2017.12.004>
- Martinez-Ibañez M, Sanchez-Diez E, Qiao LX, Meabe L, Santiago A, Zhu HJ, O'Dell LA, Carrasco J, Forsyth M, Armand M, Zhang H (2020) Weakly Coordinating Fluorine-Free Polysalt for Single Lithium-Ion Conductive Solid Polymer Electrolytes. *Batteries Supercaps* 3(8):738–746. <https://doi.org/10.1002/batt.20200045>
- Li J, Hu R, Zhou H, Tao S, Wang Y (2020) Nano-SiO<sub>2</sub>@PMMA-doped composite polymer PVDF-HFP/PMMA/PEO electrolyte for lithium metal batteries. *J Mater Sci: Mater Electron* 31(3):2708–2719. <https://doi.org/10.1007/s10854-019-02811-x>
- Kang S, Yang Z, Yang C, Zhao S, Wu N, Liu F, Chen X, Shi B (2021) Co-blending based tribasic PEO-PS-PMMA gel polymer electrolyte for quasi-solid-state lithium metal batteries. *Ionics* 27:2037–2043. <https://doi.org/10.1007/s11581-021-03964-8>
- Jin Y, Zong X, Zhang X, Liu C, Li D, Jia Z, Li G, Zhou X, Wei J, Xiong Y (2021) Interface regulation enabling three-dimensional Li<sub>1.3</sub>Al<sub>0.3</sub>Ti<sub>1.7</sub>(PO<sub>4</sub>)<sub>3</sub>-reinforced composite solid electrolyte for high-performance lithium batteries. *J Power Sources* 501: 230027. <https://doi.org/10.1016/j.jpowsour.2021.230027>
- Sedlak P, Gajdos A, Macku R, Majzner J, Holcman V, Sedlakova V, Kubersky P (2020) The effect of thermal treatment on ac/dc conductivity and current fluctuations of PVDF/NMP/[EMIM][TFSI] solid polymer electrolyte. *Sci Rep* 10(1):21140. <https://doi.org/10.1038/s41598-020-78363-6>
- Chen F, Jing M, Yang H, Yuan W, Liu M, Ji Y, Hussain S, Shen X (2021) Improved ionic conductivity and Li dendrite suppression of PVDF-based solid electrolyte membrane by LLZO incorporation and mechanical reinforcement. *Ionics* 27:1101–1111. <https://doi.org/10.1007/s11581-020-03891-0>
- Xu L, Zhang L, Hu Y, Luo L (2021) Enhancing Li-ion conduction in composite polymer electrolytes using Li<sub>0.33</sub>La<sub>0.56</sub>TiO<sub>3</sub> nanotubes. *Chem Commun* 57:11068–11071. <https://doi.org/10.1039/D1CC04220C>

21. Ren W, Ding C, Fu X, Huang Y (2021) Advanced gel polymer electrolytes for safe and durable lithium metal batteries: Challenges, strategies, and perspectives. *Energy Storage Materials* 34:515–535. <https://doi.org/10.1016/j.ensm.2020.10.018>
22. Song A, Huang Y, Zhong X, Cao H, Liu B, Lin Y, Wang M, Li X (2017) Gel polymer electrolyte with high performances based on pure natural polymer matrix of potato starch composite lignocellulose. *Electrochim Acta* 245:981–992. <https://doi.org/10.1016/j.electacta.2017.05.176>
23. Song A, Huang Y, Liu B, Cao H, Zhong X, Lin Y, Wang M, Li X, Zhong W (2017) Gel polymer electrolyte based on polyethylene glycol composite lignocellulose matrix with higher comprehensive performances. *Electrochim Acta* 247:505–515. <https://doi.org/10.1016/j.electacta.2017.07.048>
24. Li H, Xu Z, Yang J, Wang J, Hirano S (2020) Polymer electrolytes for rechargeable lithium metal batteries. *Sustainable Energy Fuels* 4(11):5469–5487. <https://doi.org/10.1039/D0SE01065K>
25. Hu P, Duan Y, Hu D, Qin B, Zhang J, Wang Q, Liu Z, Cui G, Chen L (2015) Rigid-Flexible Coupling High Ionic Conductivity Polymer Electrolyte for an Enhanced Performance of  $\text{LiMn}_2\text{O}_4/\text{Graphite}$  Battery at Elevated Temperature. *ACS Appl Mater Interfaces* 7(8):4720–4727. <https://doi.org/10.1021/am5083683>
26. Boaretto N, Meabe L, Martinez-Ibañez M, Armand M, Zhang H (2020) Review-Polymer Electrolytes for Rechargeable Batteries: From Nanocomposite to Nanohybrid. *J Electrochem Soc* 167:070524. <https://doi.org/10.1149/1945-7111/ab7221>
27. Cha JH, Didwal PN, Kim JM, Chang DR, Park C-J (2020) Poly(ethylene oxide)-based composite solid polymer electrolyte containing  $\text{Li}_7\text{La}_3\text{Zr}_2\text{O}_{12}$  and poly(ethylene glycol) dimethyl ether. *J Membr Sci* 595:117538. <https://doi.org/10.1016/j.memsci.2019.117538>
28. Niu H, Wang L, Guan P, Zhang N, Yan C, Ding M, Guo X, Huang T, Hu X (2021) Recent advances in application of ionic liquids in electrolyte of lithium ion batteries. *Journal of energy storage* 40:102659. <https://doi.org/10.1016/j.est.2021.102659>
29. Zhang D, Xu X, Qin Y, Ji S, Huo Y, Wang Z, Liu Z, Shen J, Liu J (2020) Recent progress in organic-inorganic composite solid electrolytes for all-solid-state lithium batteries. *Chem Eur J* 26:1720–1736. <https://doi.org/10.1002/chem.201904461>
30. Mayer A, Steinle D, Passerini S, Bresser D (2021) Block copolymers as (single-ion conducting) lithium battery electrolytes. *Nanotechnology* 33:062002. <https://doi.org/10.1088/1361-6528/ac2e21>
31. Kunitskaya L, Zheltonozhskaya T, Nesin S, Klepko V (2021) Polymer electrolyte membranes based on PEO-containing block copolymers. *Mol Cryst Liq Cryst* 717(1):136–142. <https://doi.org/10.1080/15421406.2020.1862456>
32. Dong L, Zeng X, Fu J, Chen L, Zhou J, Dai S, Shi L (2021) Cross-linked ionic copolymer solid electrolytes with loose Coordination-assisted lithium transport for lithium batteries. *Chem Eng J* 423:130209. <https://doi.org/10.1016/j.cej.2021.130209>
33. Shen Z, Cheng Y, Sun S, Ke X, Liu L, Shi Z (2021) The critical role of inorganic nanofillers in solid polymer composite electrolyte for  $\text{Li}^+$  transportation. *Carbon Energy* 3(3):482–508. <https://doi.org/10.1002/cey2.108>
34. Chua S, Fang R, Sun Z, Wu M, Gu Z, Wang Y, Hart JN, Sharma N, Li F, Wang D-W (2018) Hybrid Solid Polymer Electrolytes with Two-Dimensional Inorganic Nanofillers. *Chem Eur J* 24(69):18180–18203. <https://doi.org/10.1002/chem.201804781>
35. Zhang X, Daigle J-C, Zaghbi K (2020) Comprehensive Review of Polymer Architecture for All-Solid-State Lithium Rechargeable Batteries. *Materials* 13(11):2488. <https://doi.org/10.3390/ma13112488>
36. Jiang Y, Yan X, Ma Z, Mei P, Xiao W, You Q, Zhang Y (2018) Development of the PEO Based Solid Polymer Electrolytes for All-Solid State Lithium Ion Batteries. *Polymers* 10(11):1237. <https://doi.org/10.3390/polym10111237>
37. Poiana R, Lufano E, Tsurumaki A, Simari C, Nicotera I, Navarra MA (2022) Safe gel polymer electrolytes for high voltage Li-batteries. *Electrochim Acta* 401: 139470. <https://doi.org/10.1016/j.electacta.2021.139470>
38. Rong HB, Xu MQ, Xie BY, Lin HB, Zhu YM, Zheng XW, Huang WZ, Liao YH, Xing LD, Li WS (2016) A novel imidazole-based electrolyte additive for improved electrochemical performance at elevated temperature of high-voltage  $\text{LiNi}_{0.5}\text{Mn}_{1.5}\text{O}_4$  cathodes. *J Power Sources* 329:586–593. <https://doi.org/10.1016/j.jpowsour.2016.07.120>
39. Fu J, Xu Y, Dong L, Chen L, Lu Q, Li M, Zeng X, Dai S, Chen G, Shi L (2021) Multiclaw-shaped octasilsesquioxanes functionalized ionic liquids toward organic-inorganic composite electrolytes for lithium-ion batteries. *Chem Eng J* 405:126942. <https://doi.org/10.1016/j.cej.2020.126942>
40. Yu Y, Lu F, Sun N, Wu AL, Pan W, Zheng LQ (2018) Single lithium-ion polymer electrolytes based on poly(ionic liquid)s for lithium-ion batteries. *Soft Matter* 14(30):6313–6319. <https://doi.org/10.1039/c8sm00907d>
41. Ding S, Lyu Z, Niu X, Zhou Y, Liu D, Falahati M, Du D, Lin Y (2020) Integrating ionic liquids with molecular imprinting technology for biorecognition and biosensing: A review. *Biosens Bioelectron* 149:111830. <https://doi.org/10.1016/j.bios.2019.111830>
42. Huang KX, Wang YY, Mi HW, Ma DT, Yong B, Zhang PX (2020) [BMIM][BF<sub>4</sub>]-modified PVDF-HFP composite polymer electrolyte for high-performance solid-state lithium metal battery. *J Mater Chem A* 8(39):20593–20603. <https://doi.org/10.1039/d0ta08169h>
43. Sabrina Q, Sohib A, Lestariningsih T, Ratri CR (2019) The effect of ( $\text{TiO}_2$  and  $\text{SiO}_2$ ) nano-filler on solid polymer electrolyte based LiBOB. *J Phys: Conf Ser* 1191(1):012028. <https://doi.org/10.1088/1742-6596/1191/1/012028>
44. Li XL, Yang L, Shao D, Luo K, Liu L, Wu Z, Luo Z, Wang X (2020) Preparation and application of poly(ethylene oxide)-based all solid-state electrolyte with a walnut-like  $\text{SiO}_2$  as nano-fillers. *J Appl Polym Sci* 137(24):1–8. <https://doi.org/10.1002/app.48810>
45. Hema M, Tamilselvi P (2016) Lithium ion conducting PVA:PVdF polymer electrolytes doped with nano  $\text{SiO}_2$  and  $\text{TiO}_2$  filler. *J Phys Chem Solids* 96–97:42–48. <https://doi.org/10.1016/j.jpics.2016.04.008>
46. Ding S, Khan AI, Cai X, Song Y, Lyu Z, Du D, Dutta P, Lin Y (2020) Overcoming blood–brain barrier transport: Advances in nanoparticle-based drug delivery strategies. *Mater Today* 37:112–125. <https://doi.org/10.1016/j.mattod.2020.02.001>
47. Mahmoudpour M, Ding S, Lyu Z, Ebrahimi G, Du D, Dolatabadi JEN, Torbati M, Lin Y (2021) Aptamer functionalized nanomaterials for biomedical applications: Recent advances and new horizons. *Nano Today* 39:101177. <https://doi.org/10.1016/j.nantod.2021.101177>
48. Chiang CY, Reddy MJ, Chu PP (2004) Nano-tube  $\text{TiO}_2$  composite PVdF/LiPF<sub>6</sub> solid membranes. *Solid State Ionics* 175(1–4):631–635. <https://doi.org/10.1016/j.ssi.2003.12.039>
49. Marangon V, Tominaga Y, Jusef H (2020) An alternative composite polymer electrolyte for high performances lithium battery. *J Power Sources* 449:227508. <https://doi.org/10.1016/j.jpowsour.2019.227508>
50. Hou WH, Chen CY, Wang CC, Huang YH (2003) The effect of different lithium salts on conductivity of comb-like polymer electrolyte with chelating functional group. *Electrochim Acta* 48(6):679–690. [https://doi.org/10.1016/S0013-4686\(02\)00737-5](https://doi.org/10.1016/S0013-4686(02)00737-5)
51. Lin D, Liu W, Liu Y, Lee HR, Hsu P-C, Liu K, Cui Y (2016) High Ionic Conductivity of Composite Solid Polymer Electrolyte via In Situ Synthesis of Monodispersed  $\text{SiO}_2$  Nanospheres in Poly(ethylene oxide). *Nano Lett* 16:459–465. <https://doi.org/10.1021/acs.nanolett.5b04117>
52. Li J, Wu H, Ma B (2017) Preparation of bimodal mesoporous silica containing cerious salt and its application as catalyst for the



- synthesis of biodiesel by esterification. *J Porous Mater* 24:1279–1288. <https://doi.org/10.1007/s10934-017-0368-3>
53. Ding S, Zhang N, Lyu Z, Zhu W, Chang Y-C, Hu X, Du D, Lin Y (2021) Protein-based nanomaterials and nanosystems for biomedical applications: A review. *Mater Today* 43:166–184. <https://doi.org/10.1016/j.mattod.2020.11.015>
  54. Sharma J, Hashmi S (2019) Magnesium Ion-Conducting Gel Polymer Electrolyte Nanocomposites: Effect of Active and Passive Nanofillers. *Polym Compos* 40(4):1295–1306. <https://doi.org/10.1002/pc.24853>
  55. Yao P, Zhu B, Zhai H, Liao X, Zhu Y, Xu W, Cheng Q, Jayyosi C, Li Z, Zhu J, Myers KM, Chen X, Yang Y (2018) PVDF/palygorskite nanowire composite electrolyte for 4 V rechargeable lithium batteries with high energy density. *Nano Lett* 18(10):6113–6120. <https://doi.org/10.1021/acs.nanolett.8b01421>
  56. Croce F, Appetecchi GB, Persi L, Scrosati B (1998) Nanocomposite polymer electrolytes for lithium batteries. *Nature* 394:456–458. <https://doi.org/10.1038/28818>
  57. Ramesh S, Liew C-W (2012) Exploration on nano-composite fumed silica-based composite polymer electrolytes with doping of ionic liquid. *J Non-Cryst Solids* 358:931–940. <https://doi.org/10.1016/j.jnoncrysol.2012.01.005>
  58. Suthanthiraraj S, Johnsi M (2017) Nanocomposite polymer electrolytes. *Ionics* 23:2531–2542. <https://doi.org/10.1007/s11581-016-1924-6>
  59. Li B, Huang Y, Cheng P, Liu B, Yin Z, Lin Y, Li X, Wang M, Cao H, Wu Y (2019) Upgrading comprehensive performances of gel polymer electrolyte based on polyacrylonitrile via copolymerizing acrylonitrile with N-vinylpyrrolidone. *Electrochim Acta* 320:134572. <https://doi.org/10.1016/j.electacta.2019.134572>
  60. Kimura K, Matsumoto H, Hassoun J, Panero S, Scrosati B, Tomimaga Y (2015) A Quaternary Poly(ethylene carbonate)-Lithium Bis (trifluoromethanesulfonyl)imide-Ionic Liquid-Silica Fiber Composite Polymer Electrolyte for Lithium Batteries. *Electrochim Acta* 175:134–140. <https://doi.org/10.1016/j.electacta.2015.03.117>
  61. A Arya A Sharma (2017) Polymer electrolytes for lithium ion batteries: a critical study *Ionics* 23 3 497 540 <https://doi.org/10.1007/s11581-016-1908-6>
  62. Manthiram A (2011) Materials Challenges and Opportunities of Lithium Ion Batteries. *J Phys Chem Lett* 2:176–184. <https://doi.org/10.1021/jz1015422>
  63. Allen JL, Jow TR, Wolfenstine J (2011) Improved cycle life of Fe-substituted LiCoPO<sub>4</sub>. *J Power Sources* 196(20):8656–8661. <https://doi.org/10.1016/j.jpowsour.2011.06.057>
  64. Delp SA, Borodin O, Olguin M, Eisner CG, Allen JL (2016) Importance of reduction and oxidation stability of high voltage electrolytes and additives. *Electrochim Acta* 209:498–510. <https://doi.org/10.1016/j.electacta.2016.05.100>
  65. Huang J, Huang Y, Zhang Z, Gao H, Li C (2020) Li<sub>6.7</sub>La<sub>3</sub>Zr<sub>1.7</sub>Ta<sub>0.3</sub>O<sub>12</sub> reinforced PEO/PVDF-HFP based composite solid electrolyte for all solid-state lithium metal battery. *Energy Fuels* 34 (11): 15011–15018. <https://doi.org/10.1021/acs.energyfuels.0c03124>
  66. Yu X, Yu WA, Manthiram A (2021) Advances and Prospects of High-Voltage Spinel Cathodes for Lithium-Based Batteries. *Small Methods* 5(5):1–30. <https://doi.org/10.1002/smt.202001196>
  67. Praveen D, Bhat SV, Damle R (2011) Enhanced ionic conductivity in nano-composite solid polymer electrolyte: (PEG)<sub>x</sub>LiBr: y(SiO<sub>2</sub>). *Ionics* 17:21–27. <https://doi.org/10.1007/s11581-010-0476-4>
  68. Liu M, Jin B, Zhang Q, Zhan X, Chen F (2018) High-performance solid polymer electrolytes for lithium ion batteries based on sulfobetaine zwitterion and poly(ethylene oxide) modified polysiloxane. *J Alloys Compd* 742:619–628. <https://doi.org/10.1016/j.jallcom.2018.01.263>

**Publisher's note** Springer Nature remains neutral with regard to jurisdictional claims in published maps and institutional affiliations.